Light coupling and distribution for Si_3N_4/SiO_2 integrated multichannel single-mode sensing system

Andrzej Kaźmierczak
Fabian Dortu
Olivier Schrevens
Domenico Giannone, MEMBER SPIE
Multitel a.s.b.l.
B-7000 Mons, Belgium

Laurent Vivien
Delphine Marris-Morini, MEMBER SPIE
David Bouville
Eric Cassan
Université Paris-Sud 11
CNRS UMR 8622
Institut d'Electronique Fondamentale
91405 Orsay, France

Kristinn B. Gylfason
Hans Sohlström
KTH-Royal Institute of Technology
School of Electrical Engineering
Microsystem Technology Laboratory
SE-100 44 Stockholm, Sweden

Benito Sanchez
Amadeu Griol
Daniel Hill
Universidad Politécnica de Valencia
Nanophotonics Technology Center
Valencia, Spain 46022

Abstract. We present an efficient and highly alignment-tolerant light coupling and distribution system for a multichannel Si_3N_4/SiO_2 single-mode photonics sensing chip. The design of the input and output couplers and the distribution splitters is discussed. Examples of multichannel data obtained with the system are given. © *2009 Society of Photo-Optical Instrumentation Engineers.* [DOI: 10.1117/1.3067875]

Subject terms: optical systems; integrated optics; sensors; waveguides.

Paper 080811R received Oct. 13, 2008; revised manuscript received Nov. 21, 2008; accepted for publication Nov. 22, 2008; published online Jan. 26, 2009.

1 Introduction

Integrated photonics structures are advantageous for biological and chemical sensing as they can offer high sensitivity and tight integration. Numerous applications of such structures as highly integrated biosensors have been shown.[1–5] When sensor structure is integrated into multichannel photonics circuits, a multichannel biosensor can be established, allowing simultaneous detection of numerous different biomolecules. In this paper we report design and experimental evaluation of a Si_3N_4/SiO_2 planar integrated photonic circuit that can be used as a backbone of the multichannel biochemical sensor.

2 Multichannel Single-Mode Optical Sensor Chip

The principles of the multichannel single-mode optical sensor chip are schematically shown in Fig. 1. The optical signal (1) is injected to the single-input waveguide (2) and then split to multiple output waveguides in the splitting section (3). Each output waveguide is equipped with the optical sensor section (4) that typically consists of an optical resonator (microring or microdisk resonator,[1–3] Fabry–Pérot cavity,[4] Mach–Zehnder interferometer,[5] or photonics crystals cavity[6]). After passing the sensor section light is coupled out (5).

Regardless of the type of sensor, the operation of the system can be improved by improving the operation of other components of the system. In this work we focus on providing efficient and alignment-tolerant optical signal in- and out-coupling as well as on low extra loss and equilibrated signal splitting. The sensors used in our work are slot waveguide ring resonators, which have been described

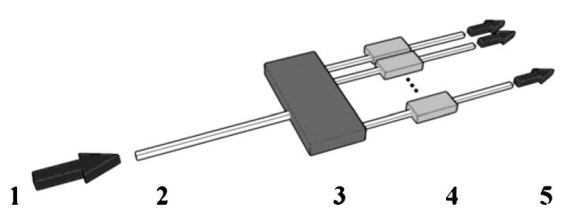

Fig. 1 Schematic representation of optical multichannel sensor.

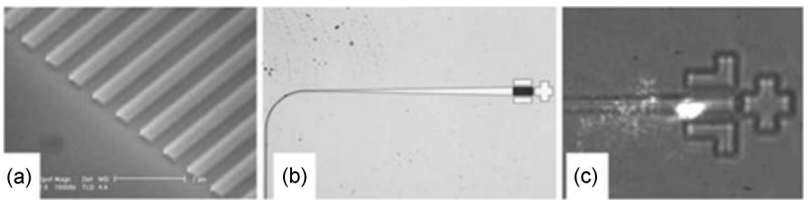

Fig. 2 Micrographs of input device in the multichannel photonics circuit: SEM close-up on surface gating coupler (a), optical microscope image of the bent input waveguide with surface grating coupler and an adiabatic taper (b). NIR image or the light input spot on surface of grating coupler (c).

elsewhere.[7] However, for completeness we show some early results obtained with microring resonators.

3 Material Choice and Waveguide Geometry

For the photonics chip we use silicon nitride, Si_3N_4, on silicon dioxide. This gives index contrast of $\Delta n \approx 0.5$, which offers a good tolerance to fabrication imperfections, low fabrication cost, and a reasonable level of integration.[8] Silicon waveguides with higher index contrast ($\Delta n \approx 2$) would allow higher integration density. However, the high optical index contrast then makes the device highly sensitive to fabrication imperfections (e.g., sidewall roughness).[9]

The experimental structures analyzed in this work were fabricated in Si_3N_4 deposited by low-pressure chemical vapor deposition (LPCVD) on a 3.3-μm-thick, thermally grown SiO_2 layer on a silicon substrate. The device layout was formed by patterning a hard mask by electron-beam lithography of PMMA, followed by chromium evaporation and lift-off. The pattern was then transferred to the Si_3N_4 layer by dry etching in He/CF_4 plasma. Finally, the devices were covered by 530 nm of silicon dioxide top cladding by tetraethyl orthosilicate LPCVD.

In the analyzed device shown in this work, we use Si_3N_4 strip waveguides with a height of 300 nm and a width of 900 nm. This allows single-mode propagation for transverse electric (TE) and transverse magnetic (TM) polarizations at a wavelength of 1.31 μm.

4 Input Coupling

The light coupling to submicrometer waveguides has been analyzed by numerous research groups. In general, two approaches to the light injection are analyzed: end-fire coupling via the photonics chip facet and surface coupling via a grating. In the first group the most noticeable solutions are 3-D[10] and inverted taper[11] coupling. In the second group, one can distinguish 1-D[12] and 2-D[13] surface grating couplers.

In the case of the analyzed multichannel optical sensor chip discussed here, the use of a 1-D surface grating input coupler was found to be the most convenient, as it provides efficient and alignment-tolerant light coupling while keeping the device size and complexity of the coupling system on a reasonable level. The coupled light is subsequently transmitted through an adiabatic taper and a bend section as shown in the scanning electron microscopy (SEM) and optical microscope images of Fig. 2.

The design of this coupler has been described in detail in Refs. 14 and 15. The main goals for the design are high efficiency and large alignment tolerance. The grating coupler was thus designed with a width as large 30 μm. The coupler exhibits an efficiency exceeding 60%, with −3 dB angular and alignment tolerances as large as 4 deg and 50 nm, respectively.

5 Output Coupling

The use of a single surface grating coupler is very convenient for the optical input coupling. However for the multiple output couplings it is difficult to use this type of device as they occupy a significant chip area. Moreover, in this case, in- and out-coupling would appear in the almost vertical direction (8–10 deg to the normal). This would make it difficult to manage the work space, as the input is usually separated from the outputs by a distance no longer than 1 cm. Further, in the case of biosensors the top surface of the photonics chip is needed for fluidic tubing or as a sample-pipetting area. These problems can be solved by out-coupling the optical signal horizontally via the end-facet of the photonic chip.

In our work, we have used inverted taper[11] output couplers as they provide efficient coupling with lower divergence and less output facet roughness influence than the conventional taper.

6 Optical Signal Splitting Strategy Choice

Optical signal splitters are one of the key components of integrated photonics. When splitters are used in cascade, they constitute an optical distribution circuit. Such networks are applied where the optical signal from one input

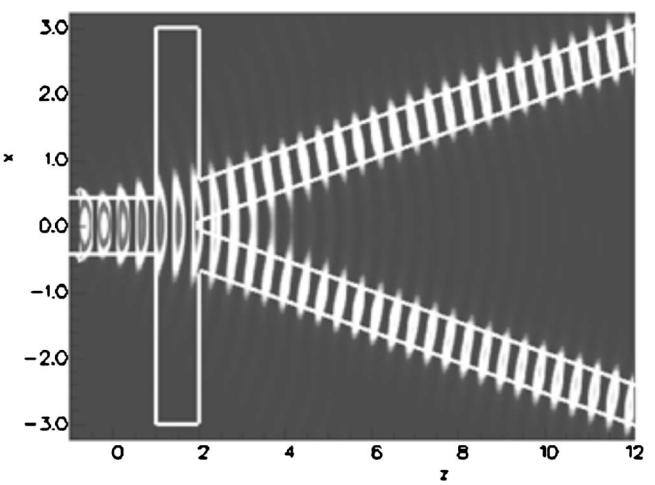

Fig. 3 2-D FDTD simulation of the electromagnetic field in the optical star splitter.

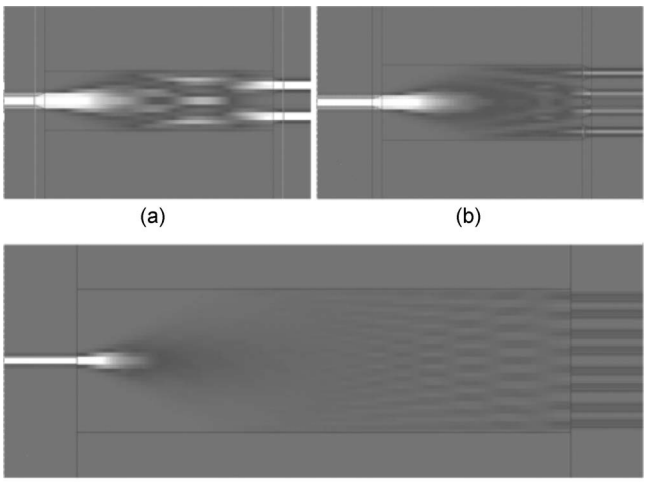

Fig. 4 FDTD 2-D simulation of the electromagnetic field in MMI splitters: (a) 1→2 MMI, (b) 2→4 MMI, and (c) 1→8 MMI.

port is delivered to several outputs (e.g., in optical clock signal distribution or optical telecommunications). Several such distribution networks using the silicon-on-insulator platform have been reported.[16–18] In our considerations we set the channel number to eight. We analyzed four different optical distribution circuits on Si_3N_4, namely, three rows of 1→2 star splitters, three rows of 1→2 multimode interference splitters (MMI), 1→4 MMI followed by a 1→2 MMI row, and finally, a single 1→8 MMI.

6.1 *Signal Splitter Simulations*

The star splitter was originally developed for silicon-on-insulator devices.[19] It is based on a free diffraction of light in an enlarged Si_3N_4 region (Fig. 3). According to the wavefront profile and the waveguide width, two output waveguides are placed to give a 1–2 splitter. With the considered waveguide geometry, such splitters are rather compact (12 μm long and 6 μm wide). Theoretical excess loss

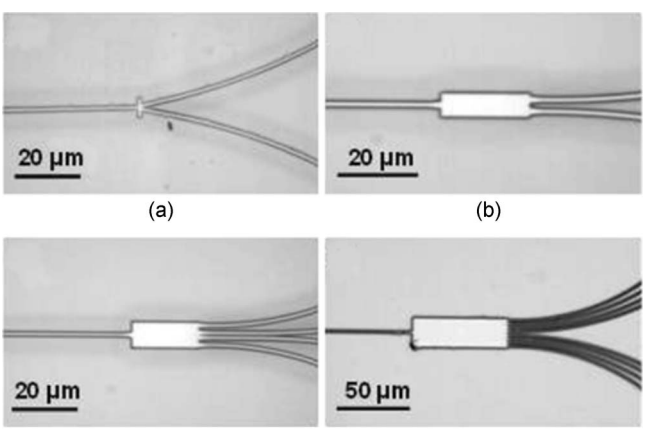

Fig. 5 Micrographs of fabricated optical signal splitters: (a) 1→2 star splitter, (b) 1→2 MMI, (c) 1→4 MMI, and (d) 1→8 MMI.

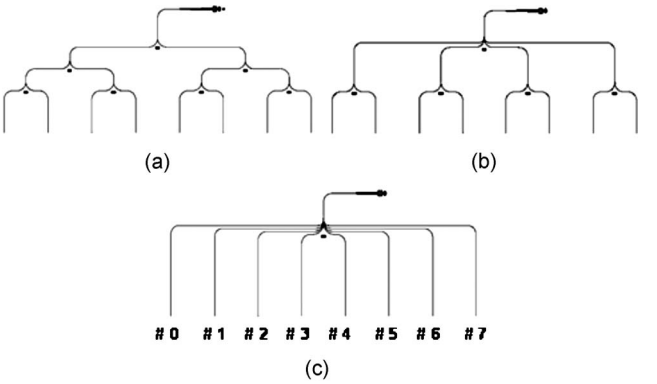

Fig. 6 Topologies of photonic integrated circuits for 1 to 8 optical signal splitting: (a) star splitter and 1→2 MMI, (b) 1→4 MMI+1→2 MMI, and (c) 1→8 MMI.

in each branch, as estimated using 2-D finite difference time domain calculations (2-D FDTD),[20,21] is less than 0.4 dB for TE polarization at 1.31 μm.

MMI splitters, in 1 to 2, 1 to 4, and 1 to 8 configurations, can also be used to distribute light to eight output points. The MMI is based on the self-imaging principle arising from multimode interference.[22] The light is launched into a multimode waveguide, and each mode propagates along the guide with its own characteristic phase velocity. At some waveguide positions, the accumulated phase differences between various excited modes are close to a multiple of 2π. Through interference, images of the input light distribution are then formed. The output waveguides are adjusted in order to obtain the best coupling. Figure 4 presents simulations of the electromagnetic field in MMI splitters, obtained using the FimmProp simulation software.[23] The length × width of 1→2, 1→4, and 1→8 MMI splitters are

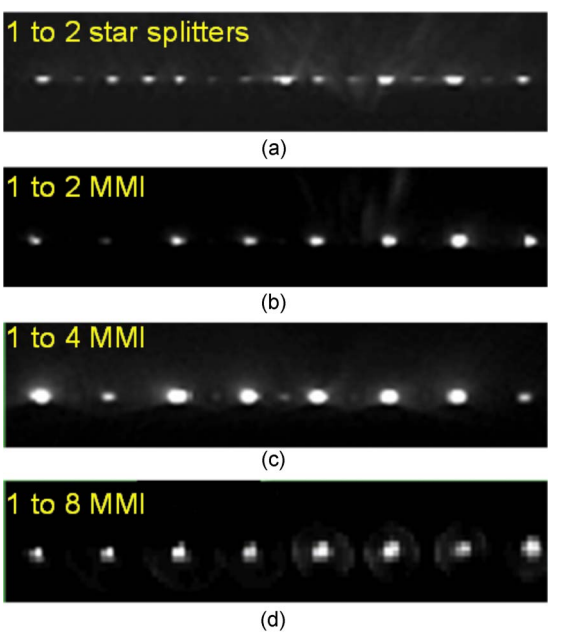

Fig. 7 NIR images of the output facet of the photonic integrated circuit with (a) 1→2 star splitters, (b) 1→2 MMIs, (c) 1→4 MMI +1→2 MMI, and (d) 1→8 MMI.

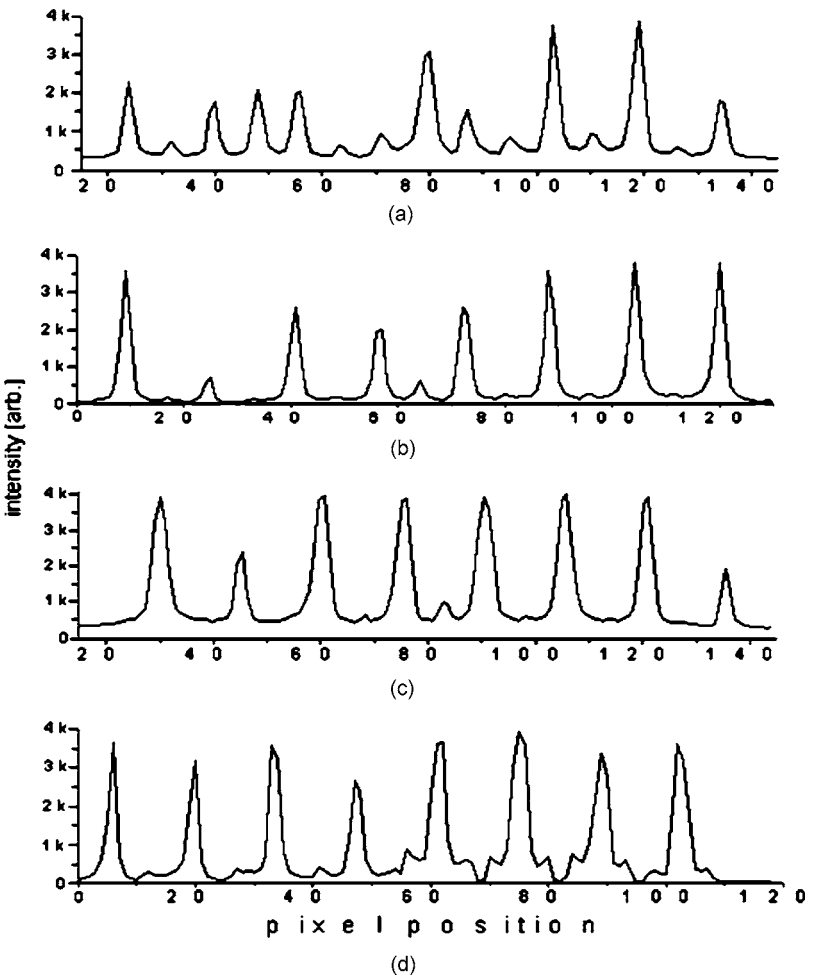

Fig. 8 Signal intensity comparison at the output of optical distribution circuit using: (a) 1→2 star splitters, (b) 1→2 MMI, (c) 1→4 MMI+1→2 MMI, and (d) 1→8 MMI.

21.5×5.6 μm, 21×8 μm, and 64×20 μm, respectively. The simulations show that the excess loss introduced by MMI splitters is equal to 0.4, 0.6, and 0.7 dB for 1→2, 1→4, and 1→8 MMI splitters, respectively.

6.2 *Distribution Circuit Topology*

Four different optical distribution circuits using the designed optical splitters were fabricated and evaluated experimentally. The analyzed circuits had the same general scheme with an input surface grating coupler and eight parallel output waveguides. When microring resonators are side coupled to the output waveguides, the circuits can be seen as functional prototypes of a multichannel sensor. Optical top-view images of the fabricated splitters are shown in Fig. 5.

Depending on the type of splitter used, the circuits were composed of one, two, or three optical splitter rows. The topologies of the analyzed optical distributions are shown schematically in Fig. 6. In the topologies presented, waveguides of different bending radius were used. In the case of topology shown in Fig. 6(a), the bending radii range from 170 to 210 μm. In the case of topologies shown in Fig. 6(b) and Fig. 6(c), radii from 100 to 290 μm are used. The sharpest waveguide bends are located at the extreme left and right outputs (nos. 0 and 7) of the 1→4 MMI +1→2 MMI and 1→8 MMI splitters.

6.3 *Distribution Circuit Experimental Characterization*

The fabricated test structures were evaluated experimentally by means of an optical setup containing a tunable laser source and a near infrared (NIR) camera. The optical signal was injected into the Si_3N_4 and collected at the output, either with the NIR camera or a photodiode detector array, to determine signal losses and distribution uniformity. NIR images of the output faces are shown in Fig. 7. As can be seen, most outputs are well-defined, but some extra light points are observed. These correspond to parasitic light leaking from the beam splitters.

Intensity profile linescans of the output facets of the test structures are shown in Fig. 8. The additional peaks appearing between those corresponding to the waveguide outputs can be seen more clearly in these graphs, especially for the star splitter circuit. The scattering at the star splitters appears to be due mainly to fabrication imperfections in the region where the two output waveguides are connected to

Table 1 Transmission loss and variance for different splitting strategies.

Distribution structure	Optical signal attenuation (dB)	Standard deviation (dB)
1→2 star splitters	36.28	2.05
1→2 MMIs	34.19	2.48
1→2 MMIs, 1→4 MMIs	29.90	1.26
1→8 MMI	28.48	0.51

the slab section. The most probable reason for the light scatter is that the silicon oxide cladding deposition may have left a void between the output waveguides of the splitter. It is also possible that random lithography errors (due to lift-off problems) or particle contamination appear, leading to random misbalance in the splitting ratio. Indeed, the proper fabrication of this region requires nanometer precision.

The devices with MMI splitters have significantly reduced this problem, and there are no significant parasitic peaks at the output of these devices. This feature is especially important for the design of photonic sensors with automated coupling, as is demonstrated below. It can also be seen that generally the MMI splitters offer better splitting uniformity.

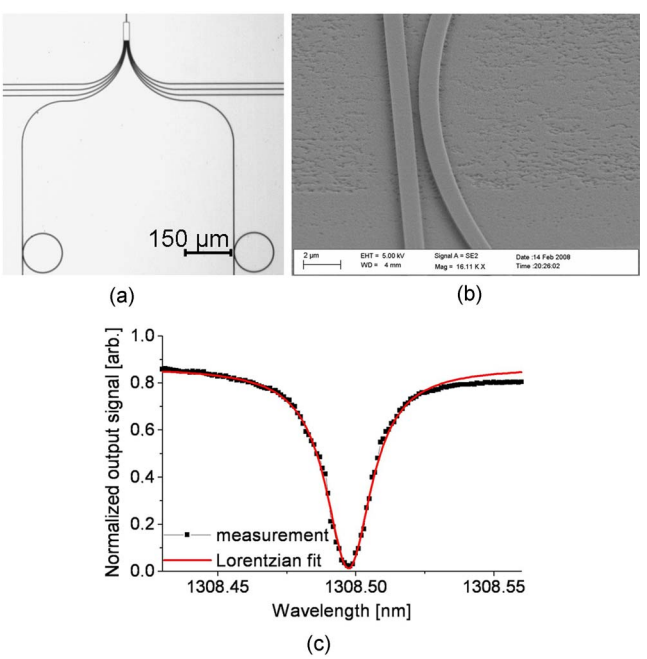

Fig. 9 Micrographs of 1→8 MMI splitter with output waveguides with side-coupled ring resonators (a) and of coupling section between microring resonator and the bus waveguide (b). Example of the wavelength spectrum of microring resonator incorporated in the optical distribution circuit (c).

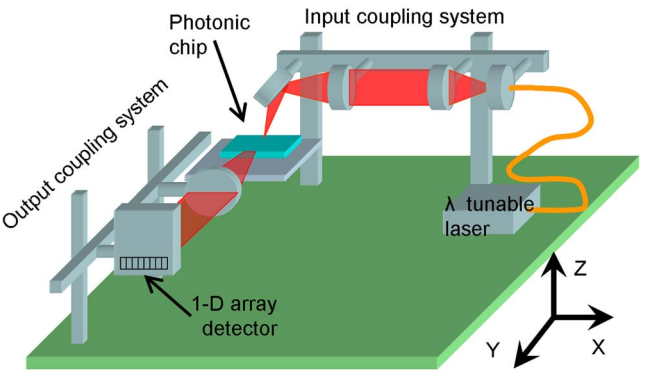

Fig. 10 Schematic representation of the experimental setup for simultaneous spectra acquisition.

The optical attenuation values measured with the photodiode detector are presented in Table 1. The measured overall attenuation values are relatively high. They correspond, however, to the total difference between the input and the output signal. Based on our knowledge of the components used, we can estimate some contributions to the loss: (*i*) propagation loss 13.6 dB/cm × 9 mm = 12.24 dB; (*ii*) insertion loss (including the loss of the surface grating) 4.6 dB; and (*iii*) signal splitting 9 dB. With optimized fabrication, input and output coupling losses as well as waveguide propagation losses are expected to decrease. Nevertheless, one can clearly observe that in the case of MMI splitters the overall loss is significantly smaller and the splitting is more uniform. The absence of parasitic light coupling from the splitters makes this coupling strategy the preferable one for photonic sensors. Furthermore, the one-stage 1 to 8 splitting with 1→8 MMI gives the lowest losses.

These experimental values can be compared to the prediction that can be made based on the known waveguide loss and the simulated performance of the splitters. This gives a predicted attenuation of about 27 dB for all the configurations. By analyzing the experimental values one can then come to the conclusion that the best and most predictable result is obtained with the one-stage splitter scheme instead of a multisplitter solution. Furthermore, one observes that there is no significant influence of the bend-

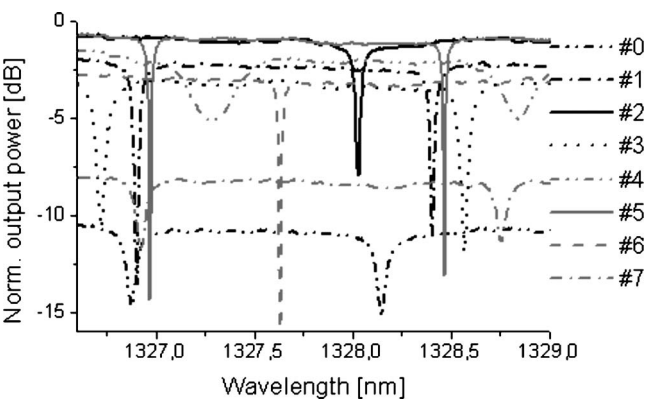

Fig. 11 Experimental results of simultaneous acquisition of transmission spectrum of eight channels of photonics integrated chip test structure.

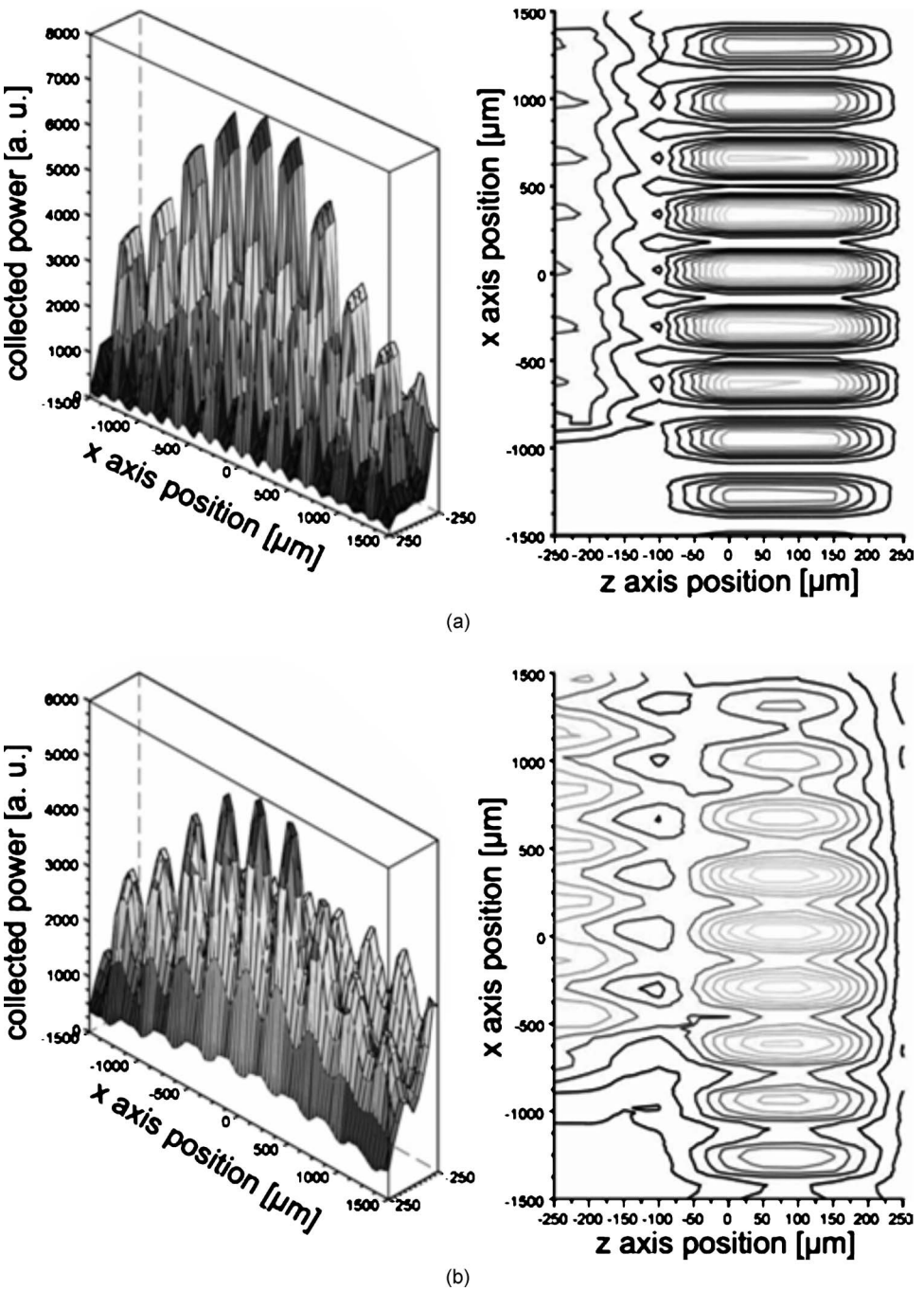

Fig. 12 2-D plot of the alignment tolerance for optical output coupling in multichannel photonics system.

ing radii on the device performance (intensity of collected signal at the nos. 0 and 7 outputs of the devices with $1 \rightarrow 4$ MMI and $1 \rightarrow 8$ MMI is not significantly worse than the one of nos. 3 and 4 outputs). Thus, one may say that for a given waveguide geometry, bending losses for the bent radius larger than 100 μm can be neglected.

7 Optical Resonators

Even though we really only discuss the light distribution scheme in this paper, we also include some information on the sensors to be able to demonstrate proper operation of the system. Each waveguide branch of the analyzed circuit was equipped with a side-coupled microring resonator. The design of these resonators has been described with detail in Ref. 24. In Fig. 9, we show an optical image of the fabricated distribution circuit, an SEM image of a microring resonator, and an example of the wavelength transmission spectrum of the resonator. The resonators were designed with different radii ranging from 80 to 120 μm, and coupling gaps between the microring and the bus waveguide ranging from 500 to 700 nm. The typical values of the quality factor varied between 20,000 and 60,000, and the

throughput attenuation at resonance varied from 10 to 25 dB. The best results were obtained for the microring resonator with a radius of 90 μm and a gap of 700 nm with a quality factor of 77,000 (intrinsic quality of 133,000) and throughput attenuation of 15.9 dB. These results provided the suitability of the technology for fabricating high-quality and possibly highly sensitive resonators.

8 Multichannel Transmission Spectrum Acquisition

To verify the operation of the multichannel photonic structure, simultaneous acquisition of wavelength spectra at eight channels was made. In order to perform such measurements an experimental setup using free space input and output optical coupling, a tunable laser source, and a 1-D InGaAs photodiode detector array was constructed. The setup configuration is shown in Fig. 10.

The experimental setup was designed to be a prototype of a simple optical platform for interrogating multichannel sensors. In order to simplify the system, the optical input path was as simple as a pair of 1-in.-diam, 100-mm working distance glass lenses and a 1-in. flat aluminum mirror. The optical platform exploited a tunable laser source working in O band (1260–1360 nm) as the photonic structures were optimized for operation at 1310 nm wavelength. The optical output path was composed of an achromatic pair objective that converted the output pitch of the photonic chip (1000 μm) to the pitch of the detector (400 μm). The exploited detector was a 1-D array of InGaAs photodiodes with a single-pixel area as large as 130 μm (width) $\times$300 μm (height). The pixel pitch of the detector was 200 μm, and as the number of the detector pixels was twice the number of the photonics chip channels, we decided to use each second pixel of the detector and therefore to use the effective pitch of 400 μm. Although the optical detector sensitivity was optimized for operating wavelength of 1700 nm, it was suitable also for the 1310 nm wavelength.

Using this setup the multichannel operation of the photonics circuits was evaluated experimentally. Examples of transmission spectra obtained are shown in Fig. 11. Transmission spectra were acquired at all channels of the photonic circuit. For each output signal the resonant wavelength can be easily resolved. It is noticeable that for the extreme left and right channels, nos. 0 and 7, the optical signal level is significantly lower. This was due to an aberration problem in the optical system that was used to adapt the output waveguide pitch of the photonic circuit (1 mm) to the pitch of the detector array (400 μm). It did not limit the possibility of reading out the resonant wavelength of these channels. Furthermore, in the case of multichannel photonic sensors the use of reference channels is strongly needed in order to increase measurement sensitivity and relax temperature stabilization constraints,[25] and the external channels can serve as a reference for normalizing the wavelength response of the other (measurement) channels.

8.1 *Alignment Tolerance of Optical Multichannel System*

After demonstrating the possibility of multichannel spectra acquisition, the optical alignment tolerance of the whole system (optical platform and photonic chip) was evaluated experimentally. The tolerance evaluation was conducted in two steps: evaluation of the output coupling tolerance and evaluation of the whole system tolerance. The input coupling tolerance is just the tolerance of the surface grating coupler that has been reported previously.[14,15]

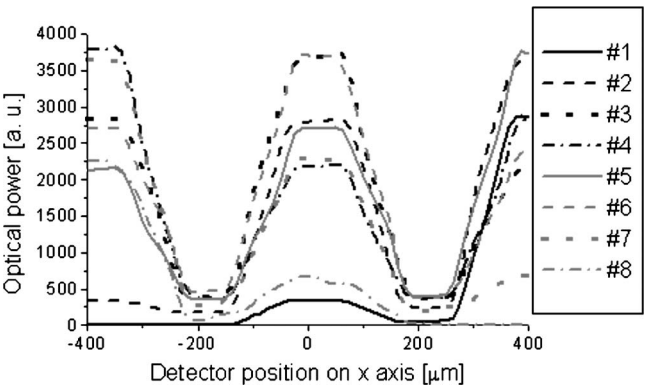

Fig. 13 Optical signal power collected by eight channels of the detector as a function of the detector shift.

In order to determine the output coupling tolerance of the system, the detector array was placed on 3-D translation stage while the input coupling was fixed using a manual setting. A 3-D scan of the output detector position was subsequently performed. The results obtained are plotted in Fig. 12 as the sum of optical power collected by the eight measurement channels of the detector versus the detector position.

The two 2-D (x, z-axis) plots are perhaps easier to interpret. In Fig. 12(a) the collected output power scan at the focal plane of the optical axis is shown. The scan along the vertical axis (z) is a visualization of the pixel height of the detector. Indeed, the signal strongly decreases as the edge of the detector reaches the spot limits. A periodic, sawlike shape along the detector axis (x) demonstrates the transition of the light coupling from active (measurement) to passive (unused) pixels. The sharper the sawlike shape, the better the alignment in the x- and z-axes. When the detector is translated by 1000 μm along the optical axis (y), the sawlike shape becomes smoother as a consequence of the defocusing of the image [Fig. 12(b)]. It is noticeable that also with such large misalignment, a significant fraction of the signal is still coupled to the detector pixels. The relation between the output alignment and the pixel size of the detector is shown in Fig. 13, showing the power collected by each detector channel as a function of the position of the detector in the x axis.

The figure confirms that the central position (x=0) corresponds to the best alignment because all channels receive an optical signal. When the detector is shifted by −200 or by +200 μm, the light is coupled to nonactive detector channels. With further shift of the detector, less and less pixels collect light from the waveguides. One sees clearly that the alignment tolerance of the output coupling is almost as large as the size of the detector pixel and does not have a significant impact of the overall tolerance of the optical system that was characterized subsequently.

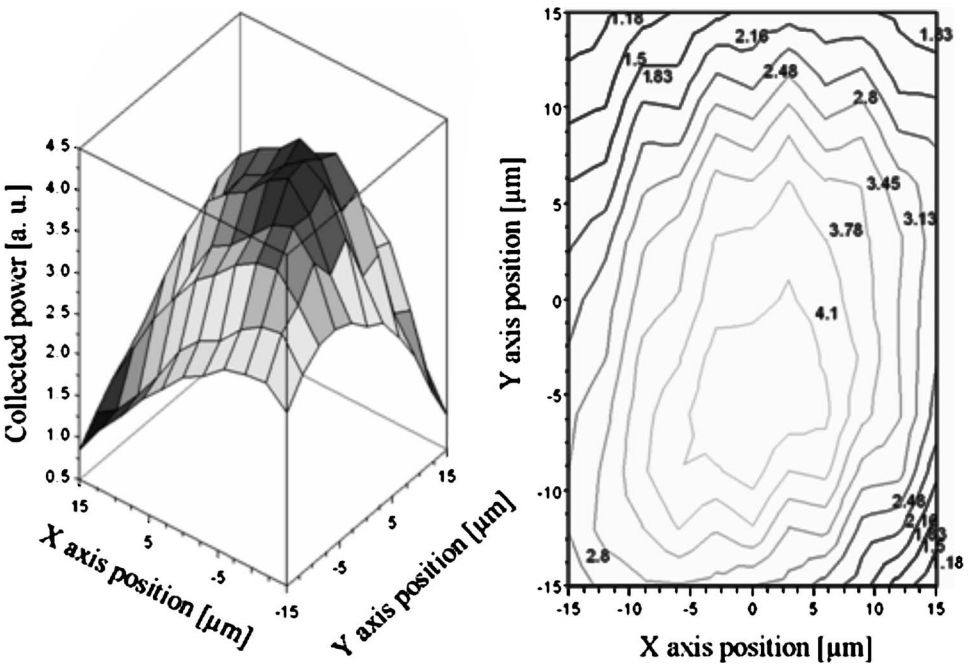

Fig. 14 Alignment tolerance of the multichannel optical system.

In order to characterize the overall alignment tolerance of the system, the 3-D motorized translation stage was placed under the photonic chip holder, enabling a 3-D scan of the photonic chip position. The results obtained are displayed in Fig. 14 as the sum of the optical signal intensity collected by eight measurement channels of the detector array versus the optical chip position. Figure 14 shows the 2-D (x- and y-axes) dependence of the collected optical signal on the photonics chip position. The obtained response is similar to the known alignment tolerance curve of the surface grating couplers. It is significant that the collected signal decreases by −3 dB when the displacement from the central (optimal) position is larger than 10 μm. With such relaxed alignment tolerance it might be possible to provide optical input and output coupling to the sensor chips without employment of any active alignment devices if package fabrication precision is at least as good as 10 μm.

9 Conclusions

We have reported design, fabrication, and characterization of a multichannel photonic circuit in the Si_3N_4/SiO_2 material platform. When equipped with appropriate optical resonators, the proposed circuit can be used as the backbone of future multichannel sensors. The use of different optical subcomponents, such as optical surface grating couplers for input coupling and inverted tapers for output coupling, was discussed. Four optical distribution circuits were analyzed, and the configuration with a unique $1 \rightarrow 8$ MMI splitter was chosen as the most profitable for the multichannel sensor circuit design. Finally, the feasibility of the analyzed circuits for multichannel measurement and its large optical alignment tolerance were demonstrated.

Acknowledgments

The authors acknowledge Suzanne Laval from IEF/CNRS for fruitful discussions. K. B. Gylfason acknowledges support of the Steinmaur Foundation, Liechtenstein. This work was done within the FP6-IST-SABIO project (Contract No. 026554), funded by the European Commission.

References

1. K. De Vos, I. Bartolozzi, D. Taillaert, W. Bogaerts, P. Bienstman, R. Baets, and E. Schacht, "Optical biosensor based on silicon-on-insolator microring cavities for specific protein detection," *Proc. SPIE*, **6447**, 6447DK (2007).
2. G.-D. Kim, G.-S. Son, H.-S. Lee, K.-D. Kim, and S.-S. Lee, "Integrated photonic glucose biosensor using a vertically coupled microring resonator in polymers," *Opt. Commun.* **281**, 4644–4647 (2008).
3. A. Schweinsberg, S. Hocdé, N. N. Lepeshkin, R. W. Boyd, C. Chase, and J. E. Fajardo, "An environmental sensor based on an integrated optical whispering gallery mode disk resonator," *Sens. Actuators B* **123**, 727–732 (2007).
4. N. Kinrot and M. Nathan, "Investigation of a periodically segmented waveguide Fabry–Pérot interferometer for use as a chemical biosensor," *J. Lightwave Technol.* **24**, 2139 (2006).
5. E. F. Schipper, A. M. Brugman, L. M. Lechuga, R. P. H. Kooyman, J. Greve, and C. Dominguez, "The realization of an integrated Mach–Zehnder waveguide immunosensor in silicon technology," *Sens. Actuators B* **40**(2–3), 147–153 (1997).
6. E. Chow, A. Grot, L. W. Mirkarimi, M. Sigalas, and G. Girolami, "Ultracompact biochemical sensor built with two-dimensional photonic crystal microcavity," *Opt. Lett.* **28**, 1093–1095 (2004).
7. C. A. Barrios, K. B. Gylfason, B. Sánchez, A. Griol, H. Sohlström, M. Holgado, and R. Casquel, "Slot-waveguide biochemical sensor," *Opt. Lett.* **32**, 3080–3082 (2007).
8. N. Daldosso, M. Melchiorri, F. Riboli, M. Girardini, G. Pucker, M. Crivellari, P. Bellutti, A. Lui, and L. Pavesi, "Comparison among various Si_3N_4 waveguide geometries grown within a CMOS fabrication pilot line," *J. Lightwave Technol.* **22**, 1734–1740 (2004).
9. F. Grillot, L. Vivien, S. Laval, D. Pascal, and E. Cassan, "Size influence on the propagation loss induced by sidewall roughness in ultrasmall SOI waveguides," *IEEE Photonics Technol. Lett.* **16**, 1661–1663 (2004).
10. M. Salib, L. Liao, R. Jones, M. Morse, A. Liu, D. Samara-Rubio, D. Alduino, and M. Paniccia, "Silicon photonics," *Intel Technol. J.* **8**, 143–160 (2004).

11. G. Roelkens, P. Dumon, W. Bogaerts, D. Van Thourhout, and R. Baets, "Efficient silicon-on-insulator fiber coupler fabricated using 248 nm deep UV lithography," *IEEE Photonics Technol. Lett.* **17**, 2613–2615 (2005).
12. L. Vivien, D. Pascal, S. Lardenois, D. Marris-Morini, E. Cassan, F. Grillot, S. Laval, J. Fédéli, and L. El Melhaoui, "Light injection in SOI microwaveguides using high-efficiency grating couplers," *J. Lightwave Technol.* **24**, 3810–3815 (2006).
13. D. Taillaert, H. Chong, P. Borel, L. Frandsen, R. M. De La Rue, and R. Baets, "A compact two-dimensional grating coupler used as a polarization splitter," *IEEE Photonics Technol. Lett.*, **15**, 1249–1251 (2003).
14. G. Maire, L. Vivien, G. Sattler, A. Kaźmierczak, B. Sanchez, K. B. Gylfason, A. Griol, D. Marris-Morini, E. Cassan, D. Giannone, H. Sohlström, and D. Hill, "High efficiency silicon nitride surface grating couplers," *Opt. Express* **16**(1), 328–333 (2008).
15. G. Maire, L. Vivien, G. Sattler, D. Marris-Morini, E. Cassan, A. Kaźmierczak, D. Giannone, B. Sanchez, A. Griol, D. Hill, K. B. Gylfason, and H. Sohlström, "High efficiency silicon nitride surface grating couplers," in *4th IEEE International Conference on Group IV Photonics*, Tokyo, 2007.
16. L. Vivien, S. Lardenois, D. Pascal, S. Laval, E. Cassan, J. L. Cercus, X. Le Roux, A. Koster, J. M. Fédéli, and M. Heitzmann, "Experimental demonstration of a low-loss optical *H*-tree distribution using silicon-on-insulator microwaveguides," *Appl. Phys. Lett.* **85**(5), 701–703 (2004).
17. D. Marris, L. Vivien, D. Pascal, M. Rouvière, E. Cassan, A. Lupu, and S. Laval, "Ultra low loss 1 to 1024 on-chip light distribution at 1.3 μm using silicon-on-insulator optical microwaveguides," *Appl. Phys. Lett.* **87**, 211102 (2005).
18. T. Fukazawa, A. Sakai, and T. Baba, "H-tree-type optical clock signal distribution circuit using a Si photonic wire waveguide," *Jpn. J. Appl. Phys., Part 2*, **41**(12B), L1461–L1463 (2002).
19. A. Koster, E. Cassan, S. Laval, L. Vivien, and D. Pascal, "Ultracompact splitter for submicrometer silicon-on-insulator rib waveguides," *J. Opt. Soc. Am. A* **21**, 2180 (2004).
20. K. Yee, "Numerical solutions of initial boundary value problems involving Maxwell's equations in isotropic media," *IEEE Trans. Antennas Propag.* **AP-14**, 302–307 (1966).
21. D. H. Choi, and W. J. R. Hoefer, "The finite-difference-time-domain method and its application to eigenvalue problems," *IEEE Trans. Microwave Theory Tech.*, **34**(12), 1464–1470 (1986).
22. Y. Ma, S. J. Park, L. W. Wang, and S. T. Ho, "Ultracompact multimode interference 3-dB coupler with strong lateral confinement by deep dry etching," *IEEE Photonics Technol. Lett.* **12**, 492–494 (2000).
23. FimmProp software, Photon Design (2008).
24. A. Kaźmierczak, L. Vivien, K. B. Gylfason, B. Sanchez, A. Griol, D. Marris-Morini, E. Cassan, F. Dortu, H. Sohlström, D. Giannone, and D. Hill, "High quality optical microring resonators in Si_3N_4/SiO_2," in *14th European Conf. on Integrated Optics ECIO 2008*, Eindhoven 2008, pp. 313—316.
25. H. Sohlström and M. Öberg, "Refractive index measurement using integrated ring resonators," *8th European Conf. on Integrated Optics ECIO 1997*, Stockholm 1997, Paper No. EThH-7.

Andrzej Kaźmierczak graduated (with honors) from the Technical University of Łodź (Poland) in 2003. He conducted his PhD research at the T. U. Łodź (Poland), and at Ecole Centrale de Lyon (France), obtaining his PhD in 2007. Currently he holds an R&D engineer position at Multitel a.s.b.l. (Mons, Belgium), coordinating Multitel activities in SABIO (Ultrahigh sensitivity Slot-wAveguide BIOsensor on a highly integrated chip for simultaneous diagnosis of multiple diseases), an EU-founded project. His scientific interests include integrated passive and active photonics devices and optical sensors. He has contributed to about 30 scientific communications in journals and at international conferences.

Fabian Dortu received his MSc in physical engineering from the Université de Liège, Belgium, in 2001. He is currently finalizing his PhD at the Katholieke Universiteit Leuven in collaboration with the Interuniversity Micro-Electronics Centre (IMEC), Leuven, working on the development of optical methods for the characterization of ultrashallow junctions. He is currently working at the Department of Applied Photonics at Multitel (Mons). His research interests include the simulation and modeling of nonlinear effects in light semiconductor interaction, planar photonics, and fiber Bragg gratings.

Domenico Giannone has been leading the Applied Photonics Department of Multitel since 2003. Before joining Multitel he was involved in several aspects of fibre Bragg grating technology and was part of the team of Dr. Raman Kashyap at British Telecom Laboratories (UK). He studied for a PhD with the Photonics Research Group, Aston University (Birmingham, UK). He is author and coauthor of more than 20 journal and conference papers on fiber lasers and fiber Bragg grating technology.

Laurent Vivien received his PhD in physics from the Polytechnique School, Palaiseau Cedex, France, in 2001. Between 2001 and 2003, he held a postdoctoral position with the Institute of Fundamental Electronics (IEF), Orsay, France, where he studied single-mode and polarization-insensitive structures in silicon-on-insulators and the coupling from submicrometric waveguides to single-mode fiber for optical telecommunication applications. Since 2003 he has joined the CNRS at the Institute of Fundamental Electronics where his activities are related to passive and active microphotonic devices on silicon for optical interconnects and optical fiber communications. Since 2006 he has been in charge of the group of Micro and Nanophotonic devices on silicon at IEF.

Kristinn B. Gylfason received his BS and MS in electrical engineering from the University of Iceland in 2001 and 2003, respectively. The spring term of 2002 he spent at the University of California, Santa Barbara, USA. From 2003 through 2005 he was a research engineer at Lyfjathroun Biopharmaceuticals, Iceland. In 2005 he received the Steinmaur Foundation nanotechnology graduate study scholarship. Since January 2006 he has been a PhD student at the Microsystem Technology Laboratory, KTH—Royal Institute of Technology, Sweden. His research has involved thin-film technology and photonic sensors for biomedical applications.

Hans Sohlström received his MSc degree in electrical engineering from the Royal Institute of Technology, Stockholm, Sweden, in 1978 and in 1993 a PhD in electrical measurement technology. The subject of his thesis was fiber optical magnetic field sensors based on YIG crystals and YIG thin films. He joined the Instrumentation Laboratory, later the Microsystem Technology group at the School of Electrical Engineering, where he is responsible for courses in measurement technology. From 1994 to 1996 he worked part-time for IMC AB, now ACREO AB, with silicon waveguiding sensors. His research interest is micro-optical sensors and other MOEMS devices. At present he is coordinating the KTH involvement in two EU-sponsored projects: SABIO and PHODYE (New PHOtonic Systems on a Chip based on DYEs for Sensor Applications scalable at Wafer Fabrication).

Amadeu Griol received telecommunication engineer and PhD degrees from the Universitat Politècnica de València in 1998 and 2003, respectively. His research interests include fabrication modeling and characterization of electrical and optical devices. His current work includes e-beam fabrication of nanodevices and nanocomponents for several optical applications, including silicon photonics and sensor technology based on silicon nitride. He has authored or coauthored more than 50 contributions to technical journals and conferences.

Daniel Hill received his BSc (Hons) in physics with astrophysics from the University of Leeds. From researching silicon-based particle detectors for his MPhil (University of Liverpool) he developed an interest in semiconductor-based materials and optoelectronics devices. After his PhD in materials science (in-situ ellipsometry monitoring of GaAs growth in chemical beam epitaxy) at the University of Liverpool, he began his silicon fabrication experience at Philips Semiconductors, Hazel Grove (UK). He has worked as a contracted postdoctoral researcher within various projects, Spanish and European, at the Universidad de Cantabria (1999–2000), Universitat Autonoma de Barcelona (2002–2004), SigmaPlus (2002–2004), and the Universitat de Barcelona (2004–2006). He joined the Universitat Politecnica de Valencia in April 2006 as senior research associate in the Nanophotonics Technology Centre (NTC) to coordinate the SABIO project and represent the NTC in the ePIXnet sensors and passive SOI device JRAs. In September 2008 he began coordinating a new FP7 ICT called 2 STReP, InTopSens. His interests are in developing new functionality in integrated photonic devices from design/fabrication/materials research, particularly for biosensors. He is a member of the Institute of Physics, a Chartered Physicist, has written several scientific papers, and regularly contributes to international conferences.

Biographies and photographs of the other authors not available.